View metadata, citation and similar papers at core.ac.uk
brought to you by CORE
provided by Brunel University Research Archive

Modelling wall shear stress in small arteries using LBM and FVM

Giuseppe PONTRELLI[1] , Carola S. KÖNIG[2], Michael W. COLLINS[3], Quan LONG[3], Sauro SUCCI[1]

*Corresponding author: Tel.: +39 0649270927; Fax: +39 064404306; Email: g.pontrelli@iac.cnr.it
1: Institute for Applied Computing, National Research Council (IAC-CNR), Italy
2: Institute for Bioengineering, Brunel University, London, UK
3: School of Engineering and Design, Brunel University, London, UK

Abstract In this study a finite-volume discretisation of a Lattice Boltzmann equation over unstructured grids is presented. The new scheme is based on the idea of placing the unknown fields at the nodes of the mesh and evolve them based on the fluxes crossing the surfaces of the corresponding control volumes. The method, named unstructured Lattice Boltzmann equation (ULBE) is compared with the classical finite volume method (FVM) and is applied here to the problem of blood flow over the endothelium in small arteries. The study shows a significant variation and a high sensitivity of wall shear stress to the endothelium corrugation degree.

Keywords: arterial endothelium, blood flow, wall shear stress, Lattice Boltzmann methods, LBM, Finite Volume Method, FVM.

1. Introduction

The flow of blood in arteries induces a viscous drag between the outermost laminae of the fluid and the vessel wall and this mechanism has a potential impact on the pathogenesis of arterial diseases. The shear stress imposed on the wall can affect the functional and structural integrity of the endothelial cells, and the possibility that such effects might be related to the development of atherosclerosis has stimulated a great deal of investigation (Nerem, 1992; Caro, 2009). Stretching of endothelial cells may modify the properties of the cell's membrane in the form of its permeability and receptors. Lesions usually occur at specific points of the arterial tree, which suggests that differences in local stress may play some role in its initialization. It is now commonly accepted that the preferred occurrence of atherosclerosis is in low wall shear regions.

Several researches concerning flows over wavy walled boundaries, both from analytical (Tsangaris and Leiter, 1984; Thomas *et al*. 2006), numerical (Sobey, 1980) and experimental (Focke, 1986) points of view have been carried out. These studies are based on a regular pattern of the wall profile, say sinusoidal or arc-shaped with different amplitudes. Most are concerned with relatively moderate and high Reynolds numbers and aim to understand transition from laminar to turbulent flow, by evidencing the formation of vortices and flow separation. In Nishimura *et al.* (1990) the characteristics of mass transfer are studied in relation to the onset of turbulence.

In this study, though, we consider the undulation of the wall as a sequence of endothelial cells with their size as obtained from the literature (Fig. 1). Only recently it has been recognized that the endothelial glycocalyx may contribute to the protection of the vascular wall in small vessels against disease by reducing friction to the flow of blood and serving as a barrier for loss of fluid through the vessel wall. Particularly in times of inflammation though, the endothelial glycocalyx is sheared off, to permit attachment of leukocytes and movement of water from microvessels resulting in the exposure of the wavy endothelium (Weinbaum *et al.*, 2003). In this work, however, only mechanical effects are considered, while all chemical and

biological processes of the endothelium are neglected. The hemodynamic problem is solved by using a Lattice Boltzmann (LB) approach (Succi, 2001). The main advantages of LB are its simplicity and amenability to parallel computing. In particular, owing to its kinetic nature, the pressure field and the stress tensor are locally available, without the need of solving any (usually expensive) Poisson problem.

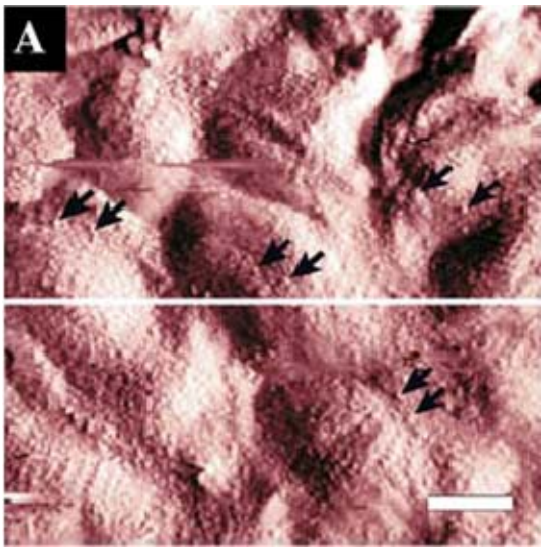

Fig. 1: The rough surface of the endothelium (from Reichlin *et al*., 2005). Arrows point to granular structures on EC's surface, white line marks scanning line for height profile evaluation, scale bar corresponds to 5μm.

Another key property of LB is that non-linearities are local (quadratic dependence of the local equilibrium on the flow field) and the non-localities are linear because advection proceeds along constant, straight lines defined by the discrete speeds. This is a very useful property, not shared by the Navier-Stokes equations, in which non-linearity and non-locality come together into the same convective term, that is, the fluid moves its own momentum along a space-time changing direction defined by the flow speed itself.
However, a recognized weakness of LB is its restriction to regular, uniform lattices (Cartesian grids). This limitation is particularly severe whenever high local resolution is required, as is the case for most flows of biomedical interest. For instance, curved boundaries must be approximated by staircase profiles aligned with the gridline coordinates, an approximation which can lead to severe inaccuracies, unless a sophisticated treatment of the boundary is devised or high grid resolution applied (Guo *et al*., 2002). The problem has motivated a wide body of research aimed at extending the LB method to non-uniform grids with boundary conditions capable of accommodating curved boundaries (Peng, 1998). Particularly interesting are recent attempts to formulate LB on fully unstructured grids using cell-vertex finite-volume schemes (Ubertini *et al*. 2002, 2004).

2. Formulation of the problem

In most studies of haemodynamics, the arterial wall is generally assumed to be flat, and the wavy surface of the endothelium is neglected: this does not imply a significant variation in the flow field, but it can be relevant in computing WSS, which is constant in a flat-walled artery. Indeed, the internal surface of the vessel wall is covered by endothelial cells that form a continuous, wavy layer. We assume that the endothelial cell membrane is solid-like, so the cells keep their shape while subjected to the shear stress due to the blood stream.
An endothelial cell (EC) has been estimated to be about 15 μm long by 0.5 μm high (Reichlin *et al*., 2005, see Fig. 1). We consider a two-dimensional channel flow between two boundary surfaces located at $y = \pm h(x)$, with the x-axis in the direction of the flow. The shape of the each internal wall appears as a smoothly corrugated surface: the channel semi-width is obtained as a perturbation around a reference value H:

$h(x) = H \pm \delta(x) = H(1 \pm \varepsilon)$ with $\varepsilon = \dfrac{\delta}{H}$ the corrugation degree.

Although the wall surface is constituted by an irregular (randomly rough) sequence of EC's, for simplicity we assume that they are regularly lined and equally distributed over the top and the bottom walls, and their size

independent of the channel height *H*. For all *H,* the aspect ratio of the channel has been fixed at 3.
The aim of this study is to investigate the dependence and the sensitivity of the WSS to the wall roughness, to the degree of corrugation and to quantify the WSS differences with the variation of vessel diameter or flow rates. Assuming axisymmetry, we limit our study to a two-dimensional straight channel, where a Newtonian fluid of viscosity μ and density ρ flows, being driven by a constant volumetric force. The fluid dynamics predictions are based on a steady flow, on the assumption that the mean flow in pulsatile conditions is similar to steady flow with the same time averaged velocity.

3. Lattice Boltzmann methodology

Let us consider the classical differential form of the single-time relaxation Lattice Boltzmann equation:

$$\partial_t f_i + \vec{c}_i \cdot \nabla f_i = -(f_i - f_i^{eq})/\lambda + F_i \qquad (1)$$

The above equation models hydrodynamic fluid flow by tracking the time-evolution of the density distribution function of pseudo-particles (or populations), defined as $f_i(\vec{x},t) \equiv f(x,\vec{v}=\vec{c}_i,t)$, where f_i is the probability of finding a particle at site $\vec{x}$, at time t moving along the lattice direction defined by the discrete speed $\vec{c}_i$. In eqn. (1) F_i represents the effect of external/internal sources of mass/momentum/energy.
The left-hand side of equation (1) represents the particle free-streaming, whereas the right-hand side represents molecular collisions via a single-time relaxation towards local equilibrium f_i^{eq} on a typical timescale λ (Benzi *et al.*, 1992).
The local equilibrium is the Maxwell-Boltzmann distribution function expanded second order in the local Mach number:

$$f_i^{eq} = \rho w_i \left[1 + \beta u_i + \frac{\beta^2}{2}(u_i^2 - u^2) \right] \qquad (2)$$

where $\beta = 1/c_s^2$, being c_s the lattice sound speed, $\rho = \sum_i f_i$ the fluid density, $\vec{u} = \sum_i \vec{c}_i f_i / \rho$ is the fluid speed and w_i are weight coefficients (normalized to unity) associated with zero-flow global equilibria.
In the limit of weak departures from local equilibrium, i.e. small Knudsen numbers, it can be shown through a Chapman-Enskog analysis that the discrete LB recovers the dynamic behaviour of a fluid with pressure $p = \rho c_s^2$ and kinematic viscosity $\nu = c_s^2(\lambda + k\Delta t)$, where k is a numerical coefficient depending on the specific time-marching scheme (*k=0* in the continuum time limit, and *k=-1/2* for the standard lattice Boltzmann equation on uniform Cartesian grids) (Benzi et al, 1992).
In order to recover the correct fluid dynamic equations in the macroscopic limit, the set of discrete speeds must satisfy mass, momentum and energy conservation, as well as rotational symmetry. It should be noted that only a limited class of lattices exhibits the right symmetry to ensure the conservation constraints. In the present work we shall refer to the two-dimensional nine-speed model (known as D2Q9) defined by the following set of discrete speeds:

$$\vec{c}_0 = (0,0),\ \vec{c}_1 = (1,0),\ \vec{c}_2 = (0,1),$$
$$\vec{c}_3 = (-1,0),\ \vec{c}_4 = (0,-1),\ \vec{c}_5 = (1,1),$$
$$\vec{c}_6 = (-1,1),\ \vec{c}_7 = (-1,-1),\ \vec{c}_8 = (1,-1).$$

with weights $w_0 = 4/9$, $w_{1\text{-}4} = 1/9$, $w_{5\text{-}8} = 1/36$ in eqn. (2). The aforementioned low-Mach number expansion restricts the use of the discrete Boltzmann equation to quasi-incompressible flows, with negligible space-time variation of the fluid density. On the other hand, since the discrete LB fluid obeys an ideal equation of state, significant pressure drops can only be sustained by supplementing/replacing the pressure gradient

with an external body force (force per unit volume) $\vec{F}$.

In a steady plane-channel flow, the magnitude of the body force is determined by imposing an exact balance with dissipative effects, i.e. $F = \mu\, \partial_{yy} u_x$. This delivers:

$$F = \frac{2\mu U_{\max}}{H^2}.$$

This approach is equivalent to assign a pressure gradient $G = \frac{2\mu U_{\max}}{H^2}$ along the channel length. The effect of the body force on the discrete populations in eqn. (1) is given by:

$F_i = \frac{w_i \vec{F} \cdot \vec{c}_i}{c_s^2}$ which finally results in the following forcing term:

$$F_i = \frac{2\lambda U_{\max}}{H^2} \qquad (3)$$

Boundary conditions are no-slip at top/bottom walls and periodic at inlet/outlet.

4. LB over unstructured grids

The presented standard LB method is macroscopically similar to a uniform Cartesian-grid solver, and this represents a severe limitation for solving complex geometries typical of haemodynamic flows. To overcome this drawback, the classical LB method has been extended to use irregular grids. This approach is based on a finite-volume scheme of the cell-vertex type consisting of a tessellation based on triangular elements. The use of unstructured grids with control volumes of arbitrary polygonal shape allows local grid refinements not possible with the standard LB. To solve eqn. (1), the nine discrete populations $f_i(\vec{x},t)$ associated to each node P of the discrete grid (Fig. 2) represent the unknowns of the problem. The finite volume over which eq. (1) is integrated is defined by means of the set of K triangles, which share P as a common vertex. Since the discrete grid is unstructured, each node is identified by its coordinates and the connectivity (P, P_k, P_k+1) is free to change from node to node. As shown in Fig.2, the portion of the control volume $\Omega_k = [C_k, E_k, P, E_{k+1}]$ that refers to the k-th triangular element is built through the union of the two sub-grid triangles $\Omega_k^- = [P, E_k, C_k]$ and $\Omega_k^+ = [P, C_k, E_{k+1}]$, where C_k is the centre of the grid element and E_k and E_k+1 are the midpoints of the edges that share P as a common vertex. Populations at off-grid points E_k and C_k are calculated with standard linear interpolations. Application of the Gauss theorem to each finite volume portion yields the following set of ordinary differential equations:

$$\partial_t f_i(P,t) = \frac{1}{V_P} \sum_k (\Phi_{ik} - \Xi_{ik}) \qquad (4)$$

where the sum $k = 0, K$ runs over the control volume $\Omega_P = \cup_k \Omega_k$ obtained by joining the centres C_k with edge midpoints E_k, V_P is the volume of Ω_P and the index $k = 0$ denotes the pivotal point P. Finally, Φ_{ik} denote the fluxes associated with streaming operator and Ξ_{ik} the integral of the collision operators of the i-th population at the k-th node, respectively. The detailed expressions of the streaming and collision matrices S_{ik} and C_{ik}, give the following general form of

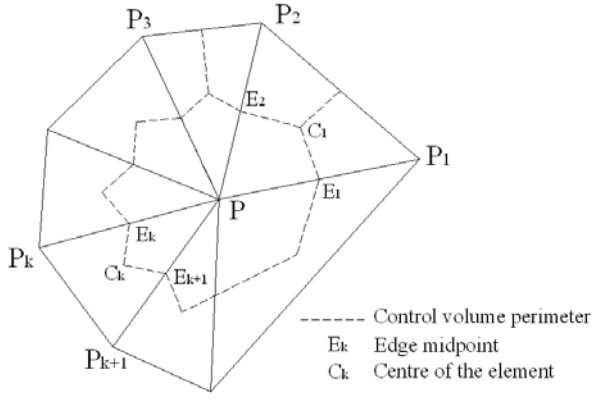

Fig. 2: The cell-vertex finite-volume discretisation around a grid point P.

the Unstructured Lattice Boltzmann Equation

(ULBE):

$$\partial_t f_i(P,t) = \sum_{k=0}^{K} S_{ik} f_i(P_k,t) - \frac{1}{\lambda}\sum_{k=0}^{K} C_{ik}[f_i(P_k,t) - f_i^{eq}(P_k,t)]$$

By definition the following sum rules apply:

$$\sum_{k=0}^{K} S_{ik} = 0, \qquad \sum_{k=0}^{K} C_{ik} = 1, \forall i$$

It is readily checked that the stress tensor $\Pi_{\alpha\beta}$ is related to the non-equilibrium component of the momentum flux tensor by the following *local* expression:

$$\Pi_{\alpha\beta} = \sum_i (f_i - f_i^{eq}) c_{i\alpha} c_{i\beta}$$

where α, β run over spatial dimensions.

5. The Finite Volume Method

In the CFD calculations a standard FVM was applied. As in the LBM model the fluid flow was treated as steady, incompressible, isothermal and Newtonian. The governing equations (continuity and momentum equations) were solved on a 2D, non-orthogonal grid using the finite volume code Ansys-CFX4. The pressure was obtained using the SIMPLE algorithm. The differencing schemes used were central differencing for pressure and hybrid differencing for the velocity variables. Appropriate scaling was achieved by applying dimensional analysis in order to achieve good convergence.

6. Computational results

First of all, a benchmark test was intended to assess the efficacy of the ULBE methodology on a flat-walled artery fully developed flow model.

We considered a uniform unstructured automatically generated grid on a 2D channel $[-3H, 3H]\times[-H, H]$, consisting of 5634 equidistributed elements, and the simulations were performed for a wide range of Reynolds numbers. Comparison of ULBE solution with the Poiseuille velocity profile:

$$u(y) = U_{\max}\left(1 - \frac{y^2}{H^2}\right) \qquad (5)$$

exhibit a maximum error $E \simeq 10^{-5}$, while the discrepancy with the wall shear stress

$$\tau = \frac{4\mu\, U_{\max}}{D} \qquad (6)$$

results of $E \simeq 10^{-4}$.

Typical values for arterioles (microcirculation) are:

$\rho = 1 g/cm^3$ μ=0.027 P

D=25 ÷ 150 μm $U_{\max} = 1 \div 40 cm/s$

that combine in a range of $\mathrm{Re} = \frac{\rho D U_{\max}}{\mu} \simeq 0.1 \div 10$. Although these values can be larger than those pertaining to the arterioles, this numerical study is aimed to understand the flow dependence on the geometrical-physical parameters on a wider range and, in particular, the sensitivity of the solution on the degree of corrugation ε and on the Reynolds number.

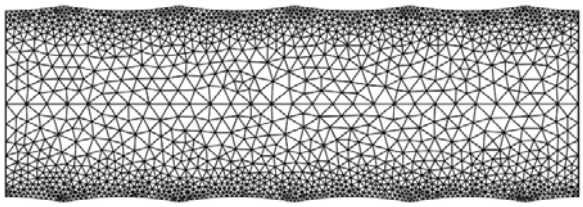

Fig. 3: The scaled 2D arterial segment covered by a refined triangular mesh.

The COMSOL package was used to generate the grid, with a mesh refinement near the wall to suit the wavy profile. For this case, the grid size ranges from 3830 (D=25) to 7960 (D=150) triangular elements. The grid is refined near the wall to suit the wavy endothelial surface (Fig. 3). The channel maximum semi-width is normalized to H=1. The time step Δt is chosen in relation to the smallest grid size (which typically reduces as H increases) in order to satisfy the CFL condition.

At such small flow rates, the velocity profiles preserve the parabolic shape (Fig. 4), but the

wall corrugation causes a local change of the velocity derivative and hence an oscillation on the WSS values. As a matter of fact, the stress has a linear rise in the transversal direction, except near the wall, where the varying cross section width generates a substantial local difference in the shear rates and stresses. Figure 5 shows that the consequence is a local variation of these quantities in a boundary layer close to the wall and an oscillation of the shear rates and WSS along the endothelium.

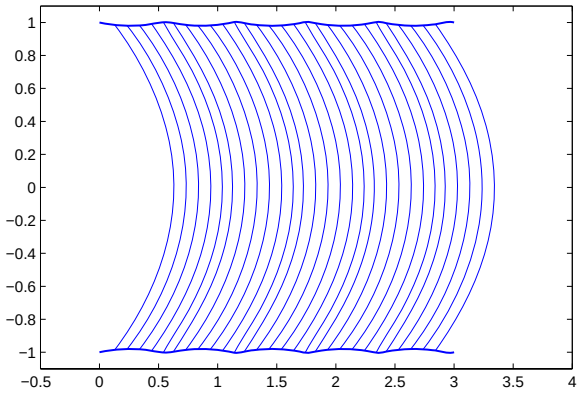

Fig. 4: Parabolic velocity profiles (x 100) along the wavy-walled channel (U=40, D=50).

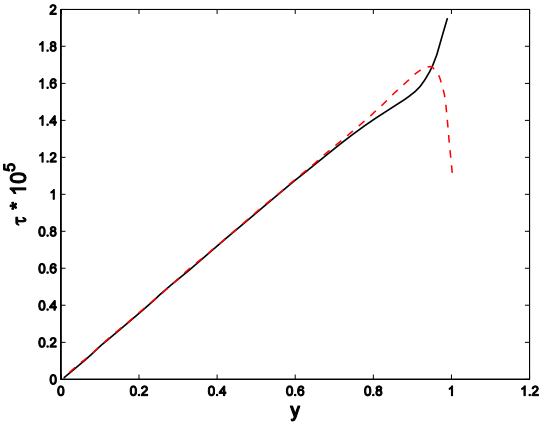

Fig. 5: Cross-stream variation of shear stress: Continuous line – peak of EC, dashed line – valley of EC (LB units).

A linear rising of the τ_+ with U is found, while an inversely linear dependence on D, as depicted in Fig. 6, describing essentially the trend of eqn. (6). A similar behaviour holds for τ_-. As a consequence, WSS oscillates between a minimum τ_- and maximum τ_+ values, which basically trace the undulation of the wall, where the minimum and maximum of τ correspond to the maximum and minimum diameters, respectively.

Table 1: The ratio τ_-/τ_+ at different velocities (cm/s) and diameters (μm). The corresponding Reynolds numbers are bracketed.

	D=25	D=50	D=100	D=150
U=1	0.55 (0.09)	0.54-0.55 (0.18)	0.55-0.56 (0.37)	0.55-0.57 (0.55)
U=20	0.55 (1.85)	0.54-0.55 (3.7)	0.55-0.56 (7.4)	0.55-0.57 (11.11)
U=40	0.55 (3.7)	0.54-0.55 (7.4)	0.55-0.56 (14.81)	0.55-0.57 (22.22)

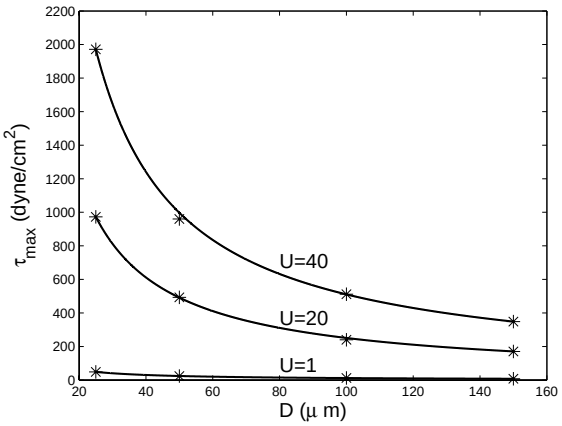

Fig. 6: Variation of the maximum wall shear stress profile for varying diameter for various maximum inlet velocities (cm/s). Stars indicate results from simulations, continuous lines are fitting curves.

Their values depends on the diameter and flow rate, but their ratio τ_-/τ_+ remains constant (Table 1). Some numerical 'wiggles' due to the grid discreteness are present in the WSS values. These minor oscillations are found to remain within a few percentage and do not play any significant role on the overall physical picture.
It is also recognized that the amplitude of the oscillating WSS can play a relevant role in the formation and development of atherosclerotic diseases. A further analysis is carried out in

this respect. In fig. 7, the linear trend of τ_+ and τ_- is shown. It is commonly accepted that critical wall shear stress levels may be those below 1Pa or above 4Pa (Atherton, 2009).

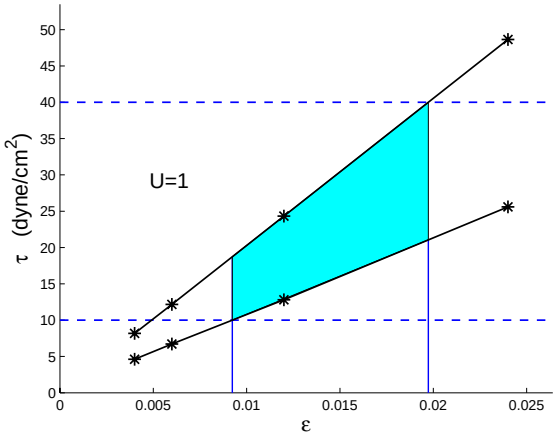

Fig. 7: The linear rise of τ_- and τ_+ with the corrugation degree ε in the case of U_{max} = 1cm/s. The shaded area depicts the safe region for corrugation degree/WSS.

Whereas FVM (König *et al.*, 1996) produced a τ_+ of 0.618 Pa (compared to a τ^* of 0.5184 Pa for straight walls) for the D = 25 μm case with U_{in} = 0.08 cm/s, the LBM method resulted in a τ_+ value of 4.864Pa, which puts both results just outside the optimal range from either end. However, this discrepancy is likely to be the result of the slightly different boundary conditions applied to the models. Whereas the FVM had a straight inlet velocity profile with a long entry length and an array of 40 ECs, the LBM model used a parabolic profile on a much shorter EC array and periodic boundary conditions. However, the results agreed favourably when the τ_-/τ_+ ratios were compared with the FVM ones being approximately 7 % lower.

Tables 2-3 show the amplitude of the oscillation $\Delta\tau/2 = (\tau_+ - \tau_-)/2$ and demonstrate the (almost) linear increasing with D. The ratio of the amplitude over the straight wall value τ^* is nearly 25% in all cases. The results show a marked variation of τ with the diameter, which increases for smaller sized arteries. Although the wall corrugation does not influence the flow pattern notably, it induces a large variation in τ.

Table 2: The amplitude of oscillation of τ and its ratio to the corresponding flat-walled value τ* at U_{max}= 1 cm/s and at several diameters.

D (μm)	ε = δ/D	Δτ /2 (dyne/cm^2)	Δτ /τ*
∞	0	0	-
150	0.0067	1.77	0.24
100	0.01	2.72	0.25
50	0.02	5.76	0.26
25	0.04	11.52	0.26

Table 3: The amplitude of oscillation of τ and its ratio to the corresponding flat-walled value τ* at U_{max}= 20 cm/s and at several diameters.

D (μm)	ε = δ/D	Δτ /2 (dyne/cm^2)	Δτ /τ*
∞	0	0	-
150	0.0067	37.33	0.25
100	0.01	55.2	0.25
50	0.02	112	0.25
25	0.04	217.6	0.25

7. Conclusion

The high sensitivity to the wall undulation supports the hypothesis for the likely onset of atheroma in small arteries. This may occur particularly in the progressed disease stages when the protective layer of the glycocalyx has been damaged or is no longer present and therefore the endothelium becomes directly exposed to the flow.

Due to some differences in the boundary conditions an explicit comparison between the LBM and FVM data is still outstanding. Further work is being developed to allow also for the comparison of 3D cases and non-Newtonian flow models.

References

Atherton, M., 2009, personal communication.

Benzi, R., Succi, S., Vergassola, M., 1992. The Lattice Boltzmann equation: theory and applications, Phys. Rep. 222; 145-197.

Caro, C.G., 2009. Discovery of the Role of Wall Shear in Atherosclerosis, Arterioscl., Thromb., and Vasc. Biol., *29*, 158-161.

Focke, W.W., Knibbe P.G., 1986. Flow visualization in parallel-plate ducts with corrugated walls, J. Fluid Mech., 165, 73-77.

Guo, Z, Zheng, C., Shu B, 2002. Discrete lattice effects on the forcing term in the lattice Boltzmann method, Phys. Rev E., 65, 046308.

Kim, S.H., Pitsch, H., 2007. A generalized periodic boundary condition for lattice Boltzmann method simulation of a pressure driven flow in a periodic geometry, Phys. Fluids, 19, 108101.

König, C.S., Long, Q. Collins, M.W., Xu, S., 2006. Numerical assessment of wall shear stress along the endothelial surface layer in small arteries . In: The Vascular Endothelium, Basic and Clinical Aspects, 6th Int. Congress, 11-12 Oct., Pisa, Italy. Abstract in Biomed. & Pharmacother. 60, 480-487.

Nannelli, F., Succi, S. 1992. The lattice Boltzmann equation in irregular lattices. J. Stat. Phys., 68, 401.

Nerem, R.M., 1992. Vascular Fluid Mechanics, the Arterial Wall, and Atherosclerosis, J. Biomech. Eng., 114(3), 274 – 283.

Nishimura, T., Murakami, S., Arakawa, S., Kawamura,Y., 1990. Flow observations and mass transfer characteristics in symmetrical wavy-walled channels at moderate Reynolds numbers for steady flows, Int. J. Heat Mass Transf., 33, 5, 835-845.

Peng, G., Xi H., Duncan, C. 1998. Lattice Boltzmann method on irregular meshes. Phys. Rev. E, 58; R4124.

Reichlin, T., Wild, A., Dürrenberger, M., Daniels, A.U., Aebi, U., Hunziker, P.R., Stolz, M., 2005. Investigating native coronary artery endothelium in situ and in cell culture by scanning force microscopy. J. Structural Biol., 152, 52-63.

Sobey, I.J., 1980. On flow through furrowed channels, part I, calculated flow patterns, J. Fluid Mech., 96, 1-26, 1980.

Succi, S., 2001. The lattice Boltzmann equation for fluid dynamics and beyond, Oxford Univ. Press, Oxford.

Thomas, A.M., Thich, G.K., Narayanan, R., 2006. Low Reynolds number flow in a channel with oscillating wavy-walls: an analytical study, Chem. Eng. Sci, 61, 6047-6056.

Tsangaris, S., E. Leiter, E., 1984. On laminar steady flow in sinusoidal channels, J. Eng. Math., 18, 89-103.

Ubertini, S., Bella G., Succi, S., 2002. Unstructured Lattice Boltzmann method: further developments, Phys. Rev. E, 68; 016701.

Ubertini, S., Succi, S., Bella, G., 2004. Lattice Boltzmann schemes without coordinates, Phil.Trans. of the Royal Society of London - Math. Phis. and Eng. Sciences, 362 (1821), 1763-1771.

Weinbaum, S., Zhang, X., Han, Y., Vink, H., and Cowin S.C., 2003. Mechanotransduction and flow across the endothelial glycocalyx, PNAS, 100(13), 7988-7995.

Xi, H., Peng, G., Chou S-H., 1999. Finite-volume lattice Boltzmann schemes in two and three dimensions. Phys. Rev. E, 60,3380.